Contract No. 777564

INNOVATIVE RUNNING GEAR SOLUTIONS FOR NEW DEPENDABLE, SUSTAINABLE, INTELLIGENT AND COMFORTABLE RAIL VEHICLES

D4.1 - Description of methods for characterizing suspension elements

Due date of deliverable: 30/11/2018

Actual submission date: 17/12/2018

Leader/Responsible of this Deliverable: Ines Lopez Arteaga, KTH Royal Institute of Technology

Reviewed: Y

Document status		
Revision	Date	Description
1	23/11/2018	First issue
2	17/12/2018	Final version after TMT approval and quality check

Project funded from the European Union's Horizon 2020 research and innovation programme		
Dissemination Level		
PU	Public	X
CO	Confidential, restricted under conditions set out in Model Grant Agreement	
CI	Classified, information as referred to in Commission Decision 2001/844/EC	

Start date of project: 01/09/2017 Duration: 24 months

REPORT CONTRIBUTORS

Name	Company	Details of Contribution
Ines Lopez Arteaga	KTH	Section 1, 3, 4, 5
Leping Feng	KTH	Section 3, 4
Leif Kari	KTH	Section 3, 4
David Thompson	ISVR	Section 1, 2, 5
Xiaowan Liu	ISVR	Section 2
Maria Laura Trifiletti	RINA- C BE	Quality check

EXECUTIVE SUMMARY

This deliverable describes the work done within Task 4.2 – Characterising suspension elements. In this task, vibration transmission through the primary suspension spring, lateral damper and traction bar is addressed. In particular, high frequency reduced order models are developed for all three components based on experimentally identified system properties. Tests are carried out on various suspension elements at the laboratories of KTH and ISVR.

For the primary suspension spring measurements for the static and dynamic stiffnesses have been carried out. The vertical static stiffness was found to be relatively constant at about 0.5 MN/m for preloads up to about 20 kN, above which it increases to about 1.4 MN/m at 39 kN. The vertical and lateral dynamic stiffnesses were measured using the indirect method with preloads applied between 10 and 40 kN. For the vertical dynamic stiffness, the magnitude at low frequencies is about 1 MN/m. There are two peaks caused by the internal resonances at around 200 and 450 Hz. Both the peak frequency and level increase with increasing preload. For the lateral stiffness, a higher magnitude tending to about 5 MN/m is found at low frequencies, and the first resonance peak occurs at around 450 Hz.

A model based on a mass-spring system including wave motion in the rubber elements has been developed. Good agreement with the measurement has been obtained for both the vertical and lateral stiffness in terms of the magnitude and the phase. Both the internal resonance frequency and the magnitude of the peak can be well predicted.

The experimental modal analysis of the traction bar based on hammer measurements and the reciprocity principle (fixed accelerometer position and moving excitation point) leads to satisfactory results. However, the loss factors found are very low, purely due to material damping, and are not representative for damping of the traction bar in the real operating conditions, where the energy losses will be dominated by the bushings and by friction at the connections.

A method for the measurement for the dynamic stiffness for rubber bushings is described and applied to the measurement of the dynamic stiffness of the bushings of the lateral damper and the traction bar. In order to obtain an estimation of the dynamic stiffness, an approximate model of the bushing is used, where the wave motion in the rubber is neglected and the bushing is modelled as a massless spring with a frequency dependent stiffness, while the casing is modelled as a massive rigid body. It is concluded that the proposed method and model lead to satisfactory estimations of the dynamic stiffness with a relatively simple measurement and calculation procedure. Therefore, the bushings of the lateral damper and traction bar can be modelled as massless springs with frequency dependent stiffness characteristics.

TABLE OF CONTENTS

LIST OF FIGURES

LIST OF TABLES

1. INTRODUCTION

This deliverable describes the work done in Task 4.2 Characterising Suspension Elements within WP4 Noise and Vibration of RUN2Rail.

The objectives of this deliverable are to measure the dynamic properties of suspension elements and propose models to describe their behaviour. The suspension elements and measured properties described in this deliverable are:

- Primary suspension spring: static and dynamic stiffness
- Bushings of the lateral damper: dynamic stiffness
- Traction bar: natural frequencies and modeshapes
- Bushings of the traction bar: dynamic stiffness.

The suspension elements studied correspond to the Metro de Madrid Series 8000 vehicle. Metro de Madrid has provided the following parts for testing:

- 1 primary suspension spring, Metro Ref. number 284321
- 1 lateral damper, Metro Ref. number 173410
- 1 traction bar, Metro Ref. number 73410
- 2 traction bar bushings, Metro Ref. number 173424

The results of this deliverable are used as input for the model built in Task 4.3 Structure-borne transmission.

2. PRIMARY SUSPENSION SPRING

2.1 INTRODUCTION

In the Metro de Madrid Series 8000 vehicles the primary suspension consists of pairs of conical rubber/metal springs at each axlebox, as shown in Figure 1. This Section of the report describes measurements of the vertical and lateral dynamic stiffness of an example primary suspension spring from this vehicle. The measurements were carried out using the indirect method [1] with a target frequency range 50 – 500 Hz. Different preloads from 10 to 40 kN were applied; this range covers the expected load range in service of 18 to 27 kN.

Results are also presented from the modelling which is developed to fit the measurement data. The model is based on a mass-spring system, initially by assuming a constant stiffness for each rubber part. It is then extended to include wave motion within the rubber elements.

Figure 1. Left, the bogie on Metro de Madrid Series 8000 vehicle. Right, the spring element used for testing is highlighted.

2.2 MEASUREMENT SET-UP

2.2.1 Measurement apparatus

The following equipment was used for the measurements:

- Electrodynamic shaker – Data Physics Corporation, model IV45, S/N 13/A6P/3O253, mass 5 kg
- Accelerometer – PCB Piezotronics Shear Accelerometer, model 352C34, sensitivity 10 mV/g
- Impact hammer – PCB Piezotronics
- Data analyser – Data Physics Corporation, model DP240, S/N 20770

The measurement setup is shown in Figure 2 along with a schematic diagram of the test rig. The spring element is located between a length of steel box section and a large steel block. For convenience it is mounted upside down. The shaft of the spring unit was recessed into a hole in the box section and attached using a large nut attached to the upper side of the box section. The lower block has dimensions 104×74×35 cm and a mass of 2050 kg. A spacer was manufactured and inserted between the spring and the lower block to allow full vertical movement. The whole rig is isolated above and below using soft rubber springs. The preload is applied by a hydraulic loading cylinder attached centrally to a steel plate, and transmitted to the upper block through the soft isolators. The tests were carried out at a temperature of approximately 20°C.

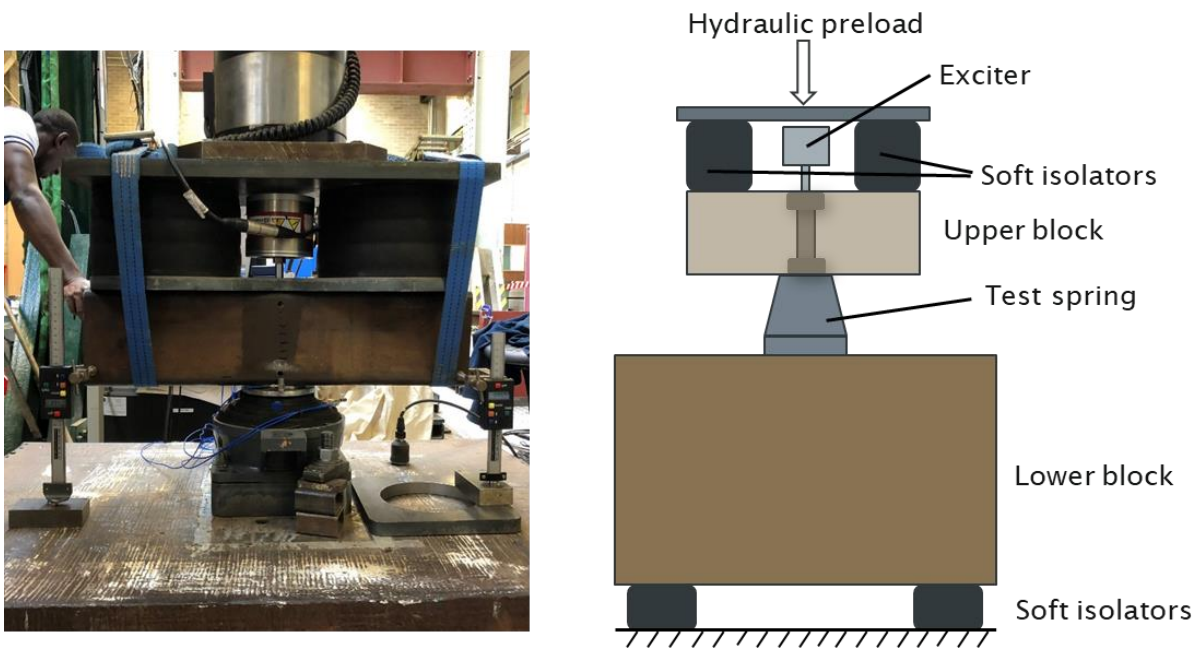

Figure 2. Measurement setup (left) and Schematic diagram of the measurement rig (right).

2.2.2 Setup for measuring static stiffness

The static stiffness was measured using the same rig setup shown in Figure 2 by applying the hydraulic preload, *F*, in steps of 2.5 kN from 2.5 kN to 45 kN. Dial gauges were attached to the two ends of the upper block, as shown in Figure 3, from which the relative displacement on each side could be read.

Figure 3. Setup for measuring static stiffness

2.2.3 Setup for measuring the vertical dynamic stiffness

Figure 4 shows the configuration used for measuring the vertical dynamic stiffness. The excitation was provided by a single electrodynamic shaker which was placed centrally on the upper block. The excitation signal was a random noise in the frequency range 10 – 1000 Hz. Different values of applied hydraulic load were used between 10 kN and 42.5 kN. The vertical vibration of the upper block is obtained by taking the average of the accelerations $\ddot{u}_1$ and $\ddot{u}_2$, which are measured using accelerometers 1 and 2 located on the top plate of the spring.

The vibration of the lower block was also recorded using two accelerometers, 3 and 4, placed on diagonally opposite sides of the spring. The average of these two signals was used to eliminate rotation of the block. The accelerometers were placed at the nodal point of the first bending mode of the block to avoid the anti-resonance in the frequency response that would otherwise occur around 500 Hz due to the effect of bending resonances.

After obtaining the vibration of the upper and lower block, the vertical dynamic stiffness can be calculated according to [2],

$$K = -m\omega^2 \left(\frac{1}{\frac{u_2+u_1}{u_3+u_4}-1} \right) \text{ for } \omega > 3\omega_1$$

where ω_1 corresponds to the natural frequency of the rigid-body mode of the lower block on the isolators.

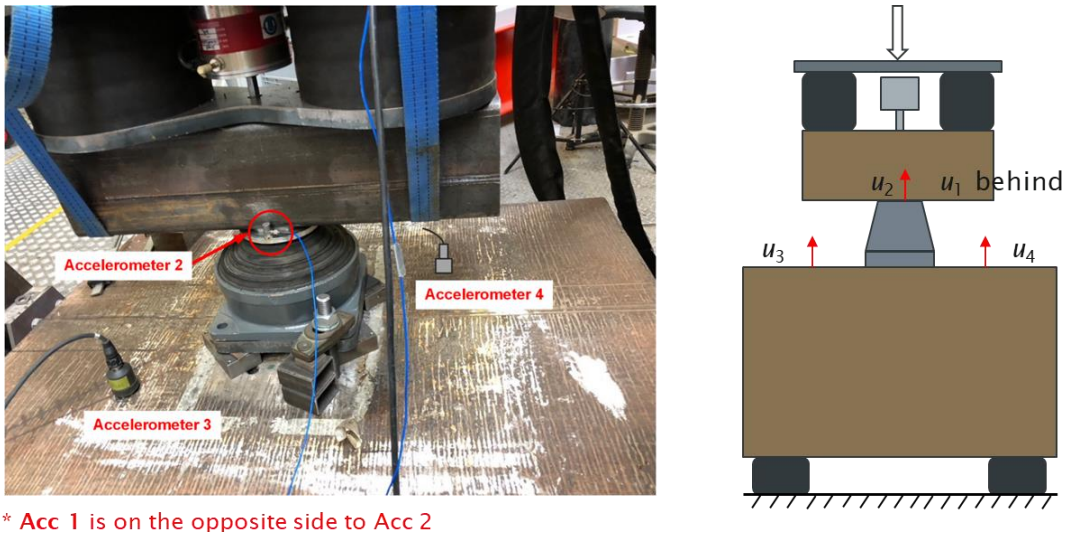

Figure 4. Locations of accelerometers (left) and the corresponding accelerations (right) for measuring the vertical dynamic stiffness.

2.2.4 Setup for measuring the lateral dynamic stiffness

For measuring the lateral dynamic stiffness, the excitation was provided by an impact hammer as this is more manageable when varying the excitation locations. In order to find the centre of rotation, seven different locations along the vertical direction were excited, which are shown in Figure 5 with the schematic diagram also given.

In order to measure the translational component of vibration, a pair of accelerometers were placed on one side of the upper block, symmetrical with respect to the centre. The difference between the two signals, was used to examine the rotation. However, the stiffness was determined using the signal from Accelerometer 2, nearest to the top of the spring. Accelerometer 3 was used to measure the lateral vibration of the lower block. The lateral complex stiffness is then given as $K = -m\omega^2\left(\frac{1}{\frac{u_2}{u_3}-1}\right)$.

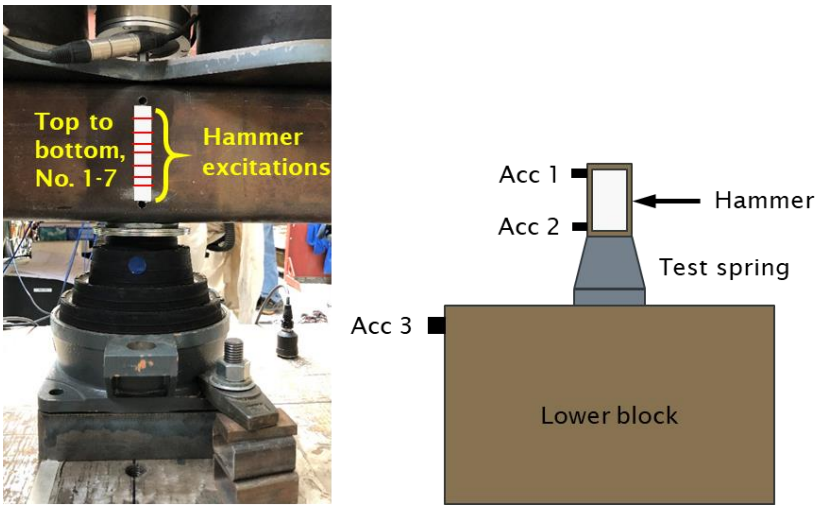

Figure 5. Locations of hammer excitations (left) and side view of the rig (right) for measuring the lateral dynamic stiffness

2.3 MEASUREMENT RESULTS

2.3.1 Static stiffness

The static load-deflection curve and the static stiffness as a function of preload are shown in Figure 6. The static stiffness is derived as $k = \Delta F/\Delta u$, where Δ indicates the relative values between the adjacent points in the load-deflection curve. It can be seen the static stiffness remains relatively constant at about 0.5 MN/m for preloads up to about 20 kN, above which it increases to about 1.4 MN/m at 39 kN.

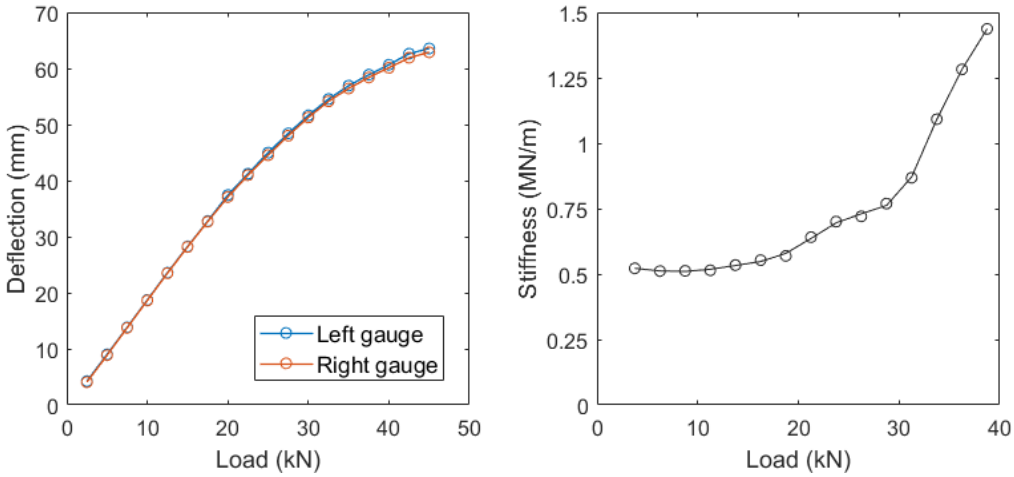

Figure 6. Static load-deflection curve (left) and static stiffness derived from it (right).

2.3.2 Vertical dynamic stiffness

The power spectral densities of the accelerations of the upper (Acc 1 and Acc 2) and lower blocks (Acc 3 and Acc 4) are shown in Figure 7 for two values of the preload. A peak between 70 and 80 Hz is found for both the upper and lower block, which corresponds to the resonance of the system with the two masses moving in anti-phase on the spring. For the lower block, there are another two peaks, at about 210 Hz and 450 Hz respectively, which are caused by the internal resonances of the spring. As the preload is increased from 20 to 30 kN, the frequencies of these peaks increase slightly.

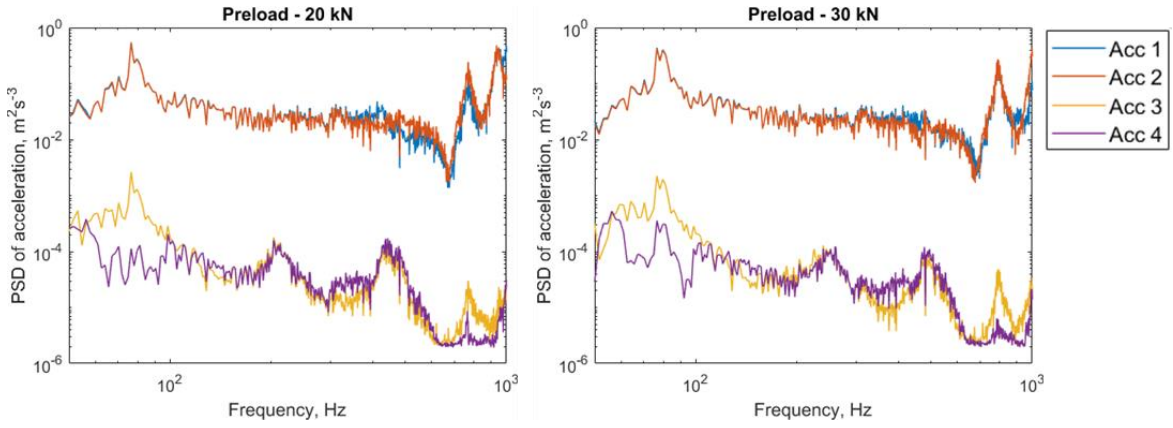

Figure 7. PSD of acceleration of upper and lower block at the preload of 20 kN (left) and 30 kN (right).

Figure 8 shows the coherence between the vibration of the upper and lower blocks. Good coherence is found for frequencies below 600 Hz for both acc 3 and acc 4 at all considered preloads. Only the results with coherence above 0.9 will be presented in the following.

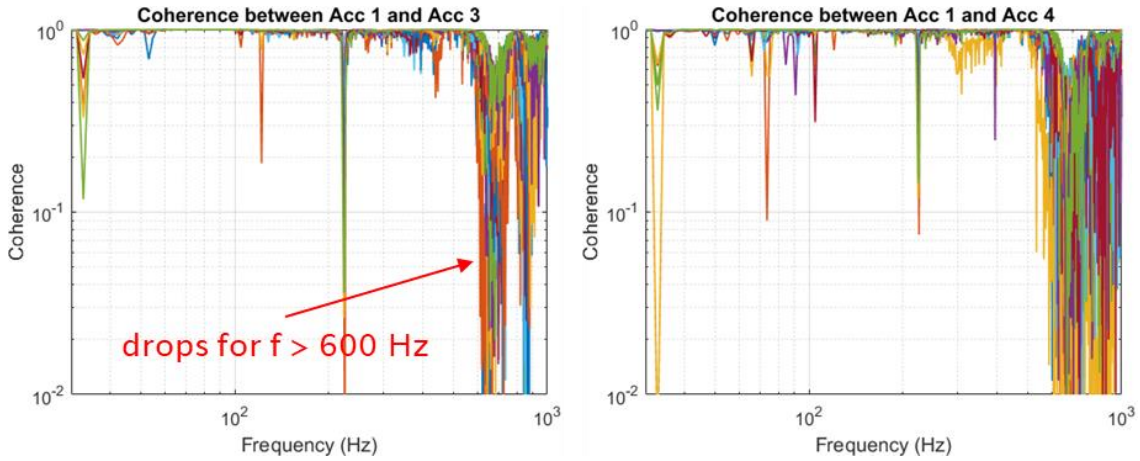

Figure 8. Coherence between accelerations on the upper and lower blocks under different preloads.

Figure 9 shows the magnitude and phase of the vertical stiffness for different preloads. At low frequencies the dynamic stiffness is around 1 to 1.5 MN/m, increasing with the preload. This is about twice the value of the static stiffness shown in Figure 6. At higher frequencies, the dynamic stiffness increases by more than a factor of 10 and the result for each preload contains three peaks, which are due to internal resonances of the spring.

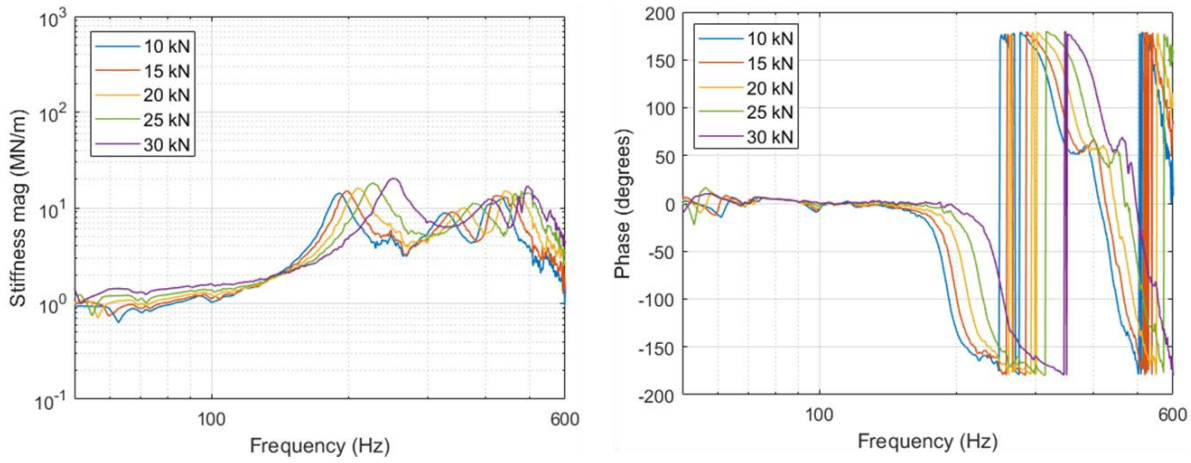

Figure 9. Magnitude and phase of complex vertical stiffness for various preloads.

2.3.3 Lateral dynamic stiffness

For lateral excitation, the coherences between the excitation force and the response at different points are displayed in Figure 10. Replacing the shaker with the hammer, the coherence at low frequency is adversely affected, with the lower limit of the usable frequency range increased to 80 Hz. The upper limit is still around 600 Hz.

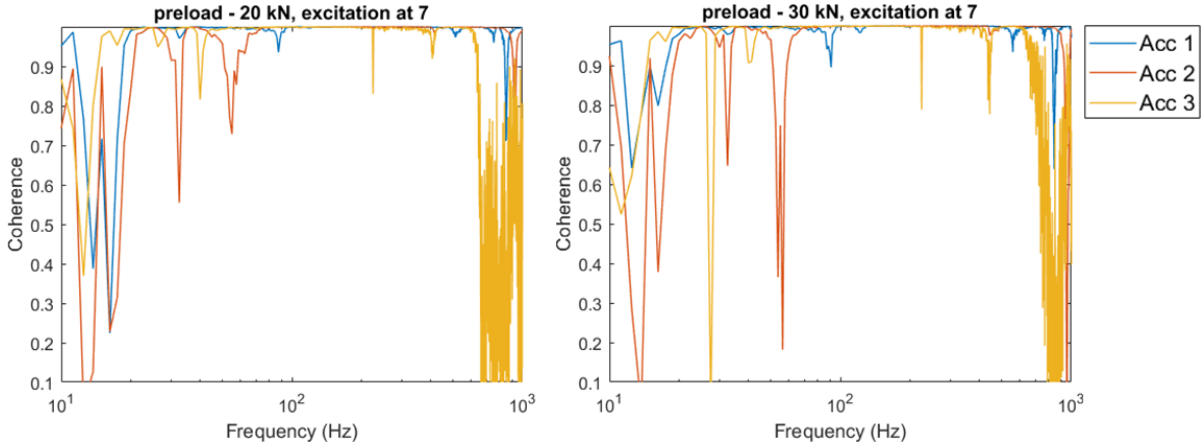

Figure 10. Coherences between hammer exciation and response at different points for preloads of 20 kN (left) and 30 kN (right).

The results for the lateral stiffness obtained for different excitation positions for the preload of 20 kN are presented in Figure 11. Although excitation was applied at different locations, there is a good consistency among the results which indicates that they are not adversely affected by rotation of the upper block. Unlike the vertical stiffness, the lateral stiffness has only a single peak which is between 400 and 500 Hz. The results below 80 Hz are not considered reliable due to the low coherence.

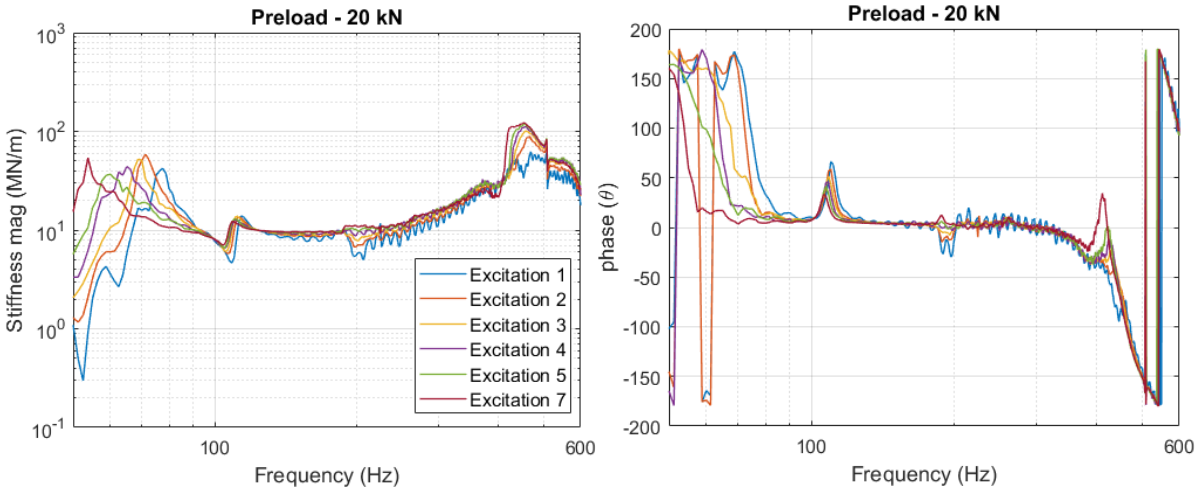

Figure 11. Magnitude and phase of complex lateral stiffness for different locations of excitations.

The lateral dynamic stiffness results obtained at the preloads of 20 and 30 kN are compared in Figure 12. With the increase in the preload, a higher amplitude is found for frequencies between 100 and 250 Hz, while the peak frequency increases slightly. Neglecting the results at low

frequency, the asymptotic value at low frequencies appears to be around 9 MN/m, which is around 10 times the value for the vertical direction.

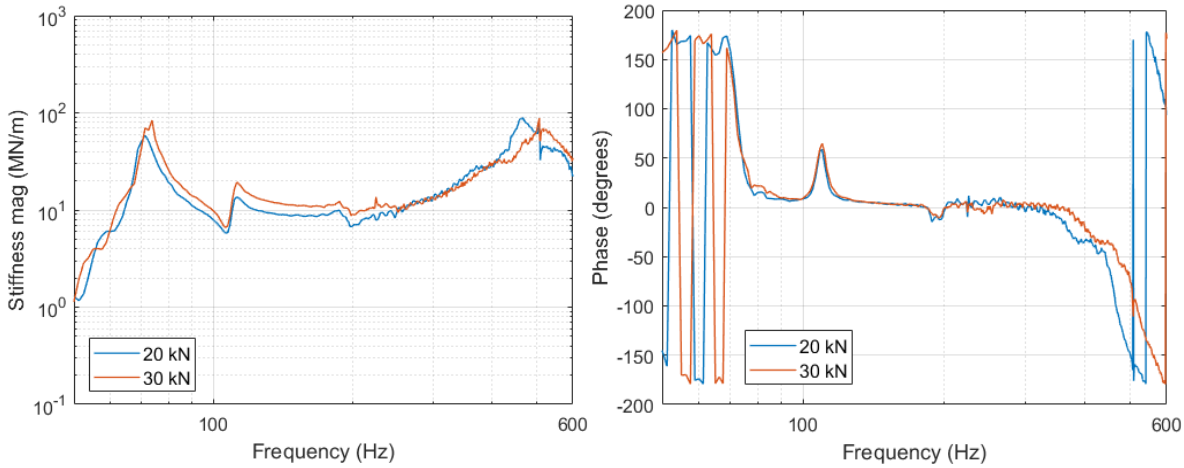

Figure 12. Magnitude and phase of complex lateral stiffness for excitation 2 at different preloads.

2.4 SPRING MODELLING METHOD AND RESULTS

2.4.1 Method

The cross-section of the spring is shown in Figure 13 (not to scale); note that here it is considered in the correct orientation, as mounted in the vehicle, whereas in the measurements described above it was mounted upside down. The area, S, of each layer of the spring, averaged between the internal and external surfaces, has been estimated and is listed in Table 1. The thickness of each rubber layer, l, and the internal metal masses, m, are also given, where m_1 refers to the inner mass, l_1 and S_1 to the thickness and area of the rubber spring between this and the next mass, etc. These parameters will be used for the modelling.

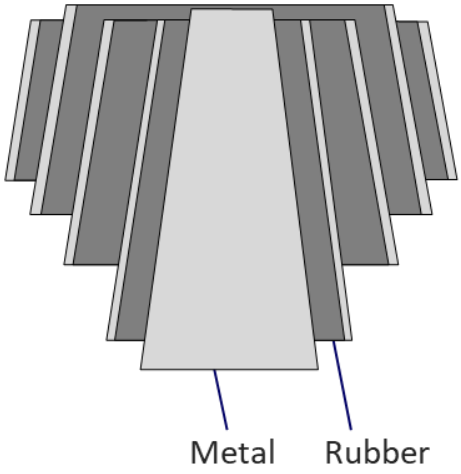

Figure 13. Cross-section of the spring (not to scale).

Table 1: Parameters of internal metal and rubber used for modelling primary suspension spring

Metal		Rubber			
m_1 (kg)	2.84	l_1 (m)	0.0183	S_1 (m^2)	0.0263
m_2 (kg)	0.82	l_2 (m)	0.0258	S_2 (m^2)	0.0336
m_3 (kg)	0.99	l_3 (m)	0.0176	S_3 (m^2)	0.0380
m_4 (kg)	1.00	l_4 (m)	0.0124	S_4 (m^2)	0.0372

Mass-spring model

The model can be expressed as a system of masses connected by four springs, as shown in Figure 14. The outer masses are excluded from the definition of the dynamic stiffness. As a first step each spring is considered to have a constant stiffness, which can satisfy the following relationship,

$$\frac{1}{K_T} = \frac{1}{K_1} + \frac{1}{K_2} + \frac{1}{K_3} + \frac{1}{K_4}$$

where K_T is the overall measured stiffness at low frequencies and K_1 etc represent the constant stiffness of each spring. By assuming that each rubber element has the same Young's modulus, the various values of constant stiffness can be determined from the above equation together with the expressions $K_1 = E_0 S_1 / l_1$ etc, where E_0 is the equivalent Young's modulus for the rubber, S is the rubber area, and l is the rubber thickness. Damping is introduced by making use of the damping loss factor η, replacing K_1 by $K_1(1+i\eta)$, etc.

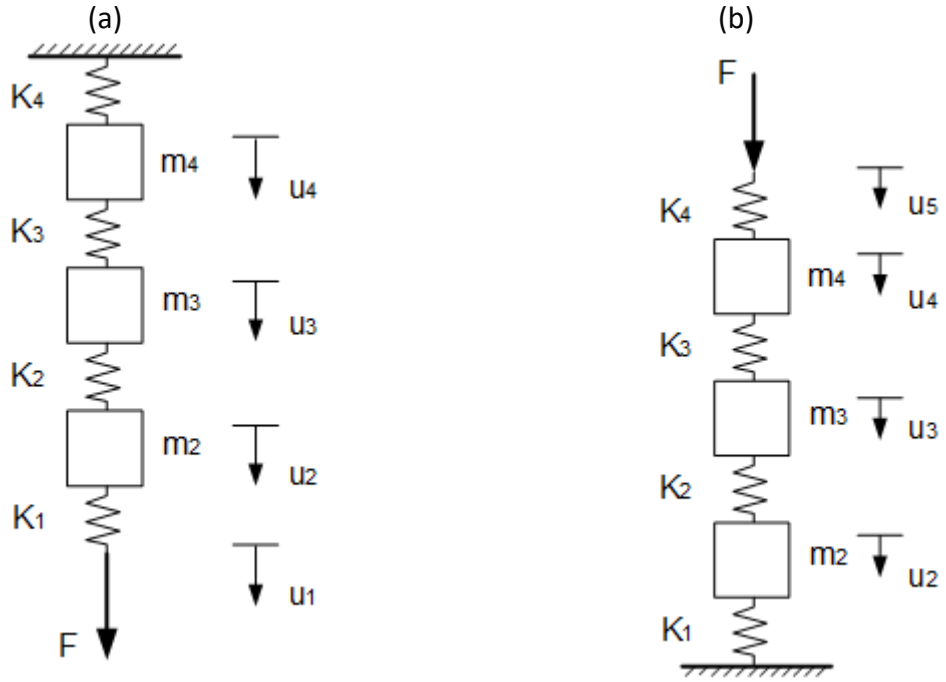

Figure 14. Equivalent mass-spring system (a) for excitation at the base (axlebox side), (b) for excitation at the top (bogie frame side)

Stiffness for excitation at the base (axlebox side)

For this mass-spring system with a unit amplitude dynamic force F=1 applied to the degree of freedom u_1, and with u_5 blocked, as shown in Figure 14(a), the equations of motion can be written in terms of matrices as given below,

Displacement vector

$$\mathbf{u} = [u_1\ u_2\ u_3\ u_4]^T$$

Stiffness matrix

$$\mathbf{K} = \begin{pmatrix} K_1 & -K_1 & 0 & 0 \\ -K_1 & K_1 + K_2 & -K_2 & 0 \\ 0 & -K_2 & K_2 + K_3 & -K_3 \\ 0 & 0 & -K_3 & K_3 + K_4 \end{pmatrix}$$

Mass matrix

$$\mathbf{M} = \begin{pmatrix} 0 & 0 & 0 & 0 \\ 0 & m_2 & 0 & 0 \\ 0 & 0 & m_3 & 0 \\ 0 & 0 & 0 & m_4 \end{pmatrix}$$

We can get

$$\mathbf{u} = (\mathbf{K} - \omega^2\mathbf{M})^{-1}[1\ 0\ 0\ 0]^T$$

The dynamic point and transfer stiffnesses for the whole system can then be derived as,

$$K_{\text{point}} = \frac{1}{u_1}$$

$$K_{\text{transfer}} = \frac{u_4 K_4}{u_1}$$

Stiffness for excitation at the top (bogie frame side)

When the spring is excited at the top, the lower degree of freedom u_1 is constrained whereas u_5 is free, as shown in Figure 14(b). The equations of motion are therefore as follows.

Displacement vector

$$\mathbf{u} = [u_2\ u_3\ u_4\ u_5]^T$$

Stiffness matrix

$$K = \begin{pmatrix} K_1 + K_2 & -K_2 & 0 & 0 \\ -K_2 & K_2 + K_3 & -K_3 & 0 \\ 0 & -K_3 & K_3 + K_4 & -K_4 \\ 0 & 0 & -K_4 & K_4 \end{pmatrix}$$

Mass matrix

$$\mathbf{M} = \begin{pmatrix} m_2 & 0 & 0 & 0 \\ 0 & m_3 & 0 & 0 \\ 0 & 0 & m_4 & 0 \\ 0 & 0 & 0 & 0 \end{pmatrix}$$

We can get

$$\mathbf{u} = (\mathbf{K} - \omega^2\mathbf{M})^{-1}[0\ 0\ 0\ 1]^T$$

and the dynamic point and transfer stiffnesses for the whole system are,

$$K_{\text{point}} = \frac{1}{u_5}$$

$$K_{\text{transfer}} = \frac{u_2 K_1}{u_5}$$

Model extension to include wave motion

Instead of using constant values for each stiffness, frequency-dependent point and transfer stiffnesses are introduced. This extension is made to include wave motion in each spring. The point and transfer stiffnesses for the rubber element 1 can be expressed as [3],

$$K_{1p} = \omega S_1 \sqrt{E\rho}\cot(kl_1) \quad \text{- point stiffness}$$
$$K_{1t} = -\omega S_1 \sqrt{E\rho}/\sin(kl_1) \quad \text{- transfer stiffness}$$

where ρ is the density, k is the wavenumber, $k = \frac{2\pi f}{c}$, where c ($= \sqrt{\frac{E}{\rho}}$) is the wave speed. Similar expressions apply to the other rubber elements.

The stiffness matrix is then modified to,

$$K = \begin{pmatrix} K_{1p} & -K_{1t} & 0 & 0 \\ -K_{1t} & K_{1p}+K_{2p} & -K_{2t} & 0 \\ 0 & -K_{2t} & K_{2p}+K_{3p} & -K_{3t} \\ 0 & 0 & -K_{3t} & K_{3p}+K_{4p} \end{pmatrix}$$

and the dynamic point and transfer stiffnesses for the whole system excited at the base are,

$$K_{\text{point}} = \frac{1}{u_1}$$

$$K_{\text{transfer}} = \frac{u_4 K_{4t}}{u_1}$$

and similarly for the stiffnesses excited at the top:

$$K_{\text{point}} = \frac{1}{u_5}$$

$$K_{\text{transfer}} = \frac{u_2 K_{1t}}{u_5}$$

2.4.2 Results

The computed transfer stiffness results obtained using the two different models, the mass-spring model and the model including wave motion, are presented in Figure 15 for the vertical stiffness and Figure 16 for the lateral stiffness, and these are compared with the measured data. Here ρ is set to 900 kg/m^3 and η is 0.12 for the rubber elements. The calculation procedure is similar for the two directions; a value of 1 MN/m is used for K_T for the vertical direction, and 5 MN/m for the lateral direction. Although the latter is smaller than the asymptotic value identified previously, it gives the best fit to the peak frequency and appears generally consistent with the results at lower frequency.

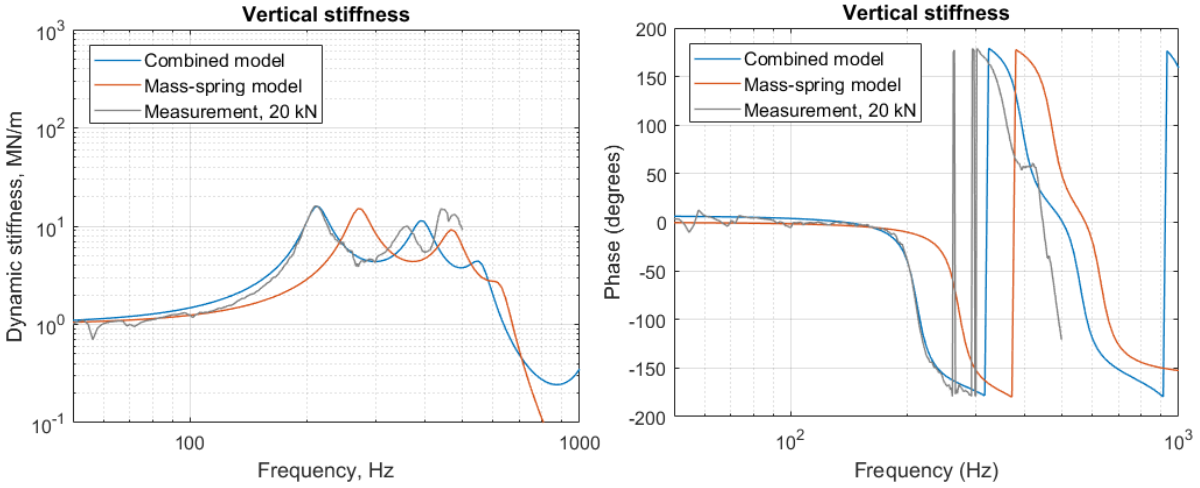

Figure 15. Comparisons between modelling and measurement for the vertical dynamic stiffness. The measurement data is from the preload of 20 kN.

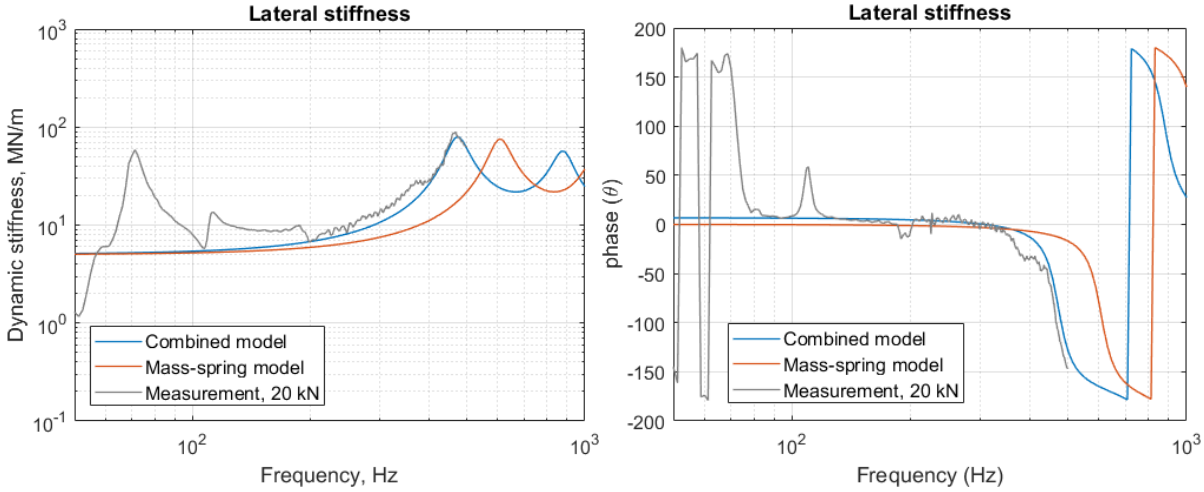

Figure 16. Comparisons between modelling and measurement for the lateral dynamic stiffness. The measurement data is from the preload of 20 kN.

As can be seen in Figure 15, for the vertical stiffness the mass-spring model based on constant stiffness values shows higher frequencies for the first and second peaks compared with the extended model and the measurement. Good agreement is obtained between the extended model and the measurement for frequencies up to 300 Hz. Both the frequency and the level of the first peak are well predicted. The second peak is also close to the measured magnitude although the frequency is higher in the modelling. Good agreement is also found for the phase by using the combined model.

The combined model also provides a good prediction for the lateral stiffness in terms of both the magnitude and the phase. Good agreement is obtained for the internal resonance frequency and the peak level although the magnitude at low frequencies, f < 200 Hz, is slightly lower in the modelling.

The model can also be used to obtain the point stiffnesses at both ends of the spring. These are shown in Figure 17 together with the transfer stiffness.

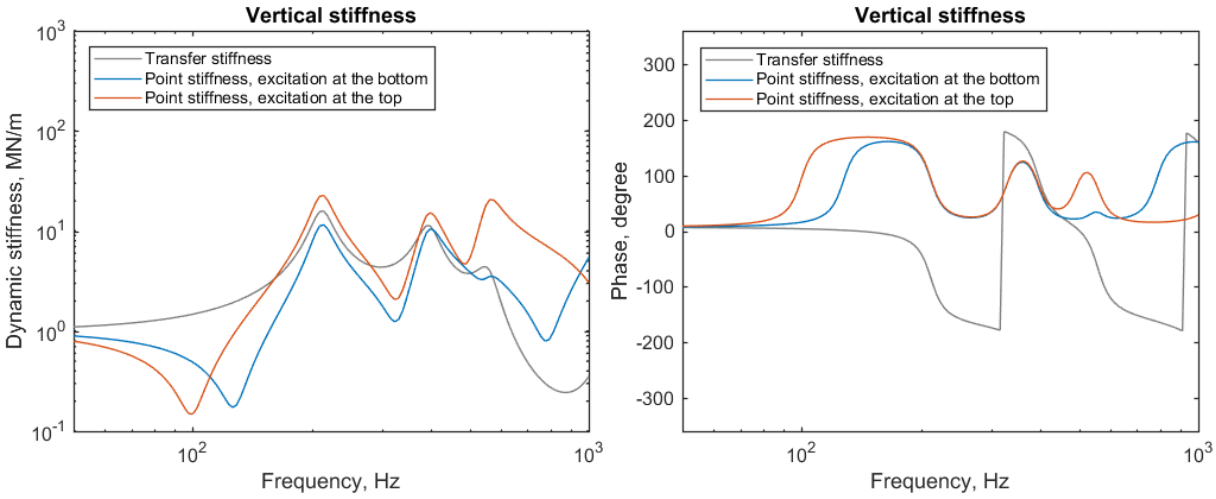

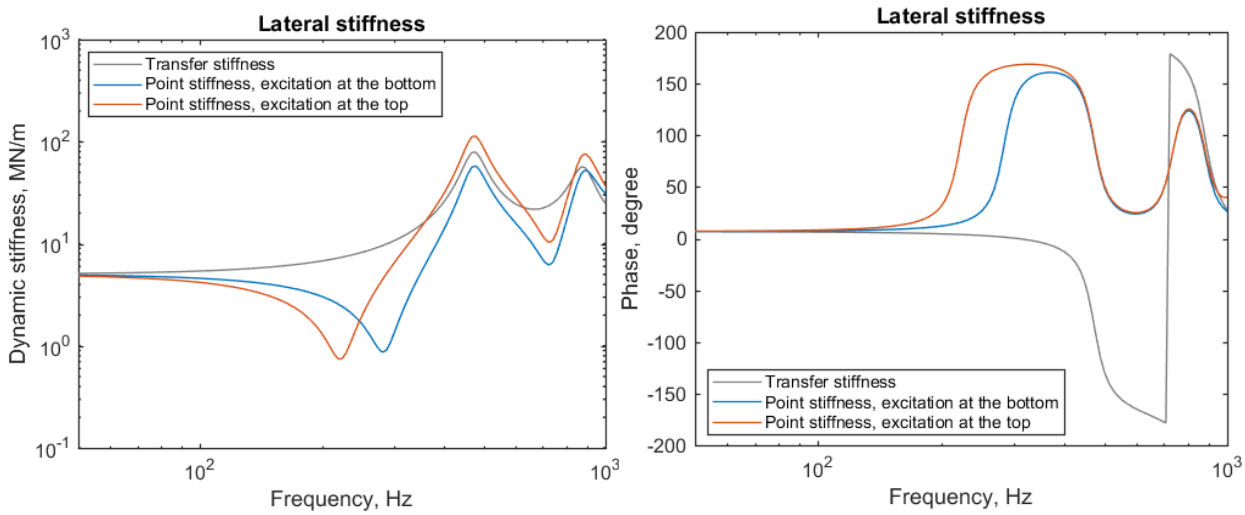

Figure 17. Vertical and lateral point and transfer dynamic stiffnesses obtained from the model.

2.5 CONCLUSIONS

Measurements for the static and dynamic stiffnesses have been carried out for the primary suspension spring from the Metro de Madrid Series 8000 vehicle. The static stiffness was found to be relatively constant at about 0.5 MN/m for preloads up to about 20 kN, above which it increases to about 1.4 MN/m at 39 kN. The vertical and lateral dynamic stiffnesses were measured using the indirect method with preloads applied between 10 and 40 kN. For the vertical dynamic stiffness, the magnitude at low frequencies is about 1 MN/m. There are two peaks caused by the internal resonances at around 200 and 450 Hz. Both the peak frequency and level increase with increasing preload. For the lateral stiffness, a higher magnitude of about 5 MN/m is found at low frequencies, and the first resonance peak occurs at around 450 Hz.

A model based on a mass-spring system including wave motion in the rubber elements has been developed. Good agreement with the measurement has been obtained for both the vertical and lateral stiffness in terms of the magnitude and the phase. Both the internal resonance frequency and the magnitude of the peak can be well predicted.

3. LATERAL DAMPER BUSHINGS

3.1 INTRODUCTION

In this section the estimation procedure for the dynamic stiffness of the bushings of the lateral damper in the Metro de Madrid Series 8000 vehicle is discussed. First the measurement method is presented, followed by a description of the experimental set-ups and the discussion of the results.

The bushings of the lateral damper are located at both ends of the damper. In this project it is assumed that these two, nominally identical, bushings have the same dynamic stiffness and, therefore, only the bushing shown in Figure 18 has been measured.

Figure 18: Close-up of one of the bushings on the lateral damper

3.2 MEASUREMENT METHOD

The method for the experimental estimation of the transfer dynamic stiffness of the bushings is based on the measurement method presented in [4], where an indirect method is proposed for the measurement of transfer dynamic stiffness of vibration isolators in the audible frequency range, up to 1000 Hz. The measurement method is illustrated in Figure 19, where methods for the estimation of the transfer dynamic stiffness in the transversal (X,Y-)directions, Figure 19(a), and axial (Z-)direction, Figure 19(b), are provided.

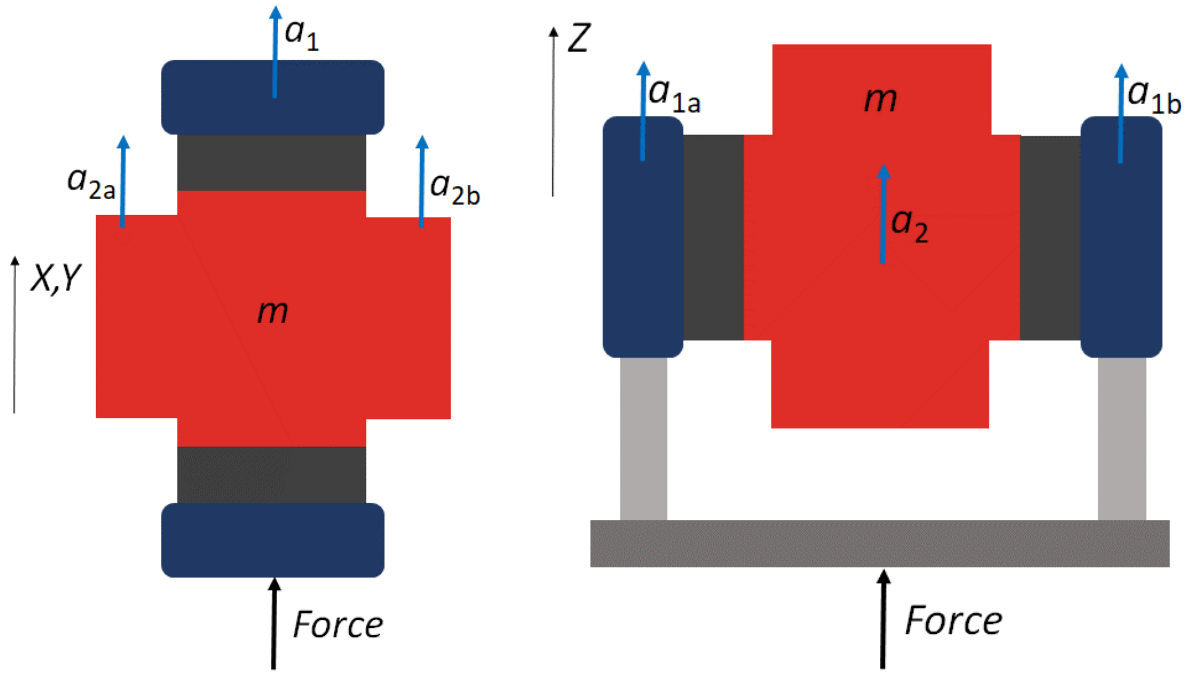

(a) (b)

Figure 19: Schematic illustration of the measurement method for dynamic stiffness estimation. (a) X and Y-direction, (b) Z-direction. m: mass of the shaft, a_1: acceleration of the casing, a_2: acceleration of the shaft.

In Figure 19, m is the mass of the shaft, a_1 is the acceleration of the casing and a_2 is the acceleration of the shaft. To compensate for possible rotational vibrations during the measurement, the acceleration of the shaft in the measurements in X,Y direction (Figure 19(a)) and the casing in the measurement in Z direction (Figure 19(b)) are measured at two symmetrically chosen positions and the acceleration in Z (or X,Y) direction of the shaft (or casing) is obtained as the average of these two measurements. Finally, in order to distribute the excitation uniformly on the circumference of the casing in the measurements in Z direction (Figure 19(b)), a hollow cylinder is attached to the casing, a transversal rod is subsequently glued to the cylinder and the force is applied in the middle of the rod.

The expressions derived in [4] include the influence of the standing-waves that appear inside the isolator at high frequencies. However, it can be shown that for sufficiently thin isolators (thickness smaller than the wavelength), the standing waves can be neglected and the isolator can be regarded as an ideal massless spring with frequency-dependent stiffness properties. In that case, an equivalent mass-spring model can be used to describe the dynamic behaviour of the bushings as illustrated in Figure 20.

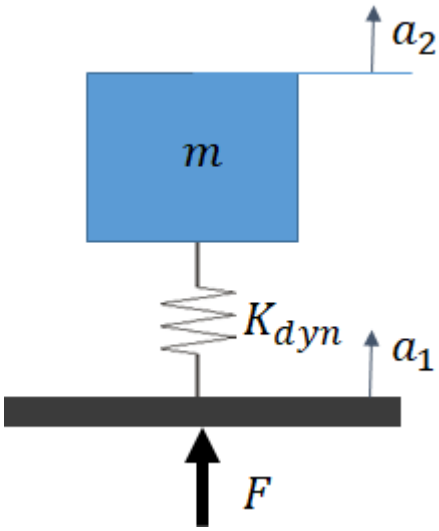

Figure 20: Equivalent mass-spring model of the bushing

In Figure 20 K_{dyn} is the frequency dependent complex dynamic stiffness of the isolator, m is the loading mass and a_1, a_2 are the accelerations on the excitation and response side respectively. It can be shown that the dynamic stiffness of the bushing can be calculated with the following expression:

$$K_{dyn} = \frac{\omega^2 mT}{T-1}, with\ T = \frac{H_{a_{2F}}}{H_{a_{1F}}}$$

and H_{a_2F}, H_{a_1F} the transfer functions between the excitation force and the accelerations on the response and excitation side, respectively.

3.3 MEASUREMENT SET-UP

3.3.1 Measurement apparatus

The following equipment is used for the measurements;

- Electrodynamic shaker – Ling Dynamic type V408, S/N 53537-5
- Power amplifier – B&K type 2706, S/N 660122
- Force transducer – B&K type 8200, S/N 1895664
- Accelerometers – B&K type 4394V (2.4 g), S/N 1929297 and 2127840
- Charge amplifiers – B&K type 2635, S/N 1799669, 1117816 and 638484
- 4-ch. Signal analyzing system Siglab, DSP Technology, S/N 11315

The measurements are performed with the stepped sine method, i.e., excitation and measurements are performed at a single tone at a time, in the frequency range 30 Hz – 800 Hz. The frequency step is 1 Hz between 30 and 400 Hz, and is 4 Hz between 400 and 800 Hz. In total 471 frequency points are measured.

The mass of the shaft is calculated to be 0.9 kg from the geometry of the shaft and by assuming a material density of 7850 kg/m^3

3.3.2 Set-up for the measurement of the lateral dynamic stiffness

The set-up for the measurement of the lateral dynamic stiffness is shown in Figure 21.

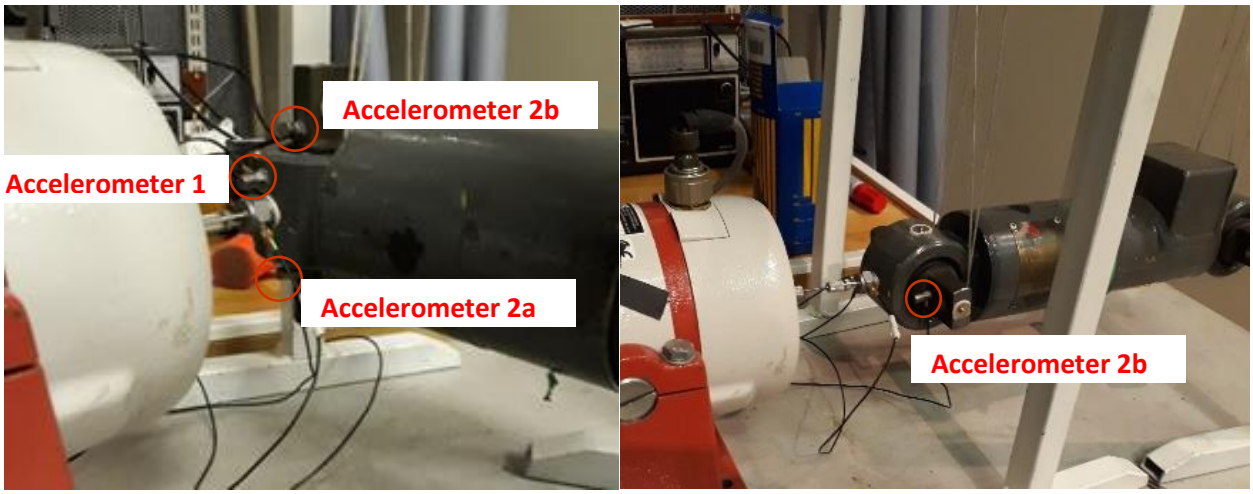

(a) (b)

Figure 21: Dynamic stiffness measurements in (a) X- direction and (b) Y-direction. The acceleration of the shaft is measured with two accelerometers (2a and 2b) to compensate for rotation.

The excitation position and the positions of accelerometers 1, 2a and 2b can be seen in Figure 21(a) for the measurement in the X-direction. A similar configuration is used for the measurement in the Y-direction, Figure 21(b), although only accelerometer 2b is visible.

3.3.3 Set-up for the measurement of the axial dynamic stiffness

The set-up for the measurements of the dynamic stiffness in the axial (Z) direction can be seen in Figure 22.

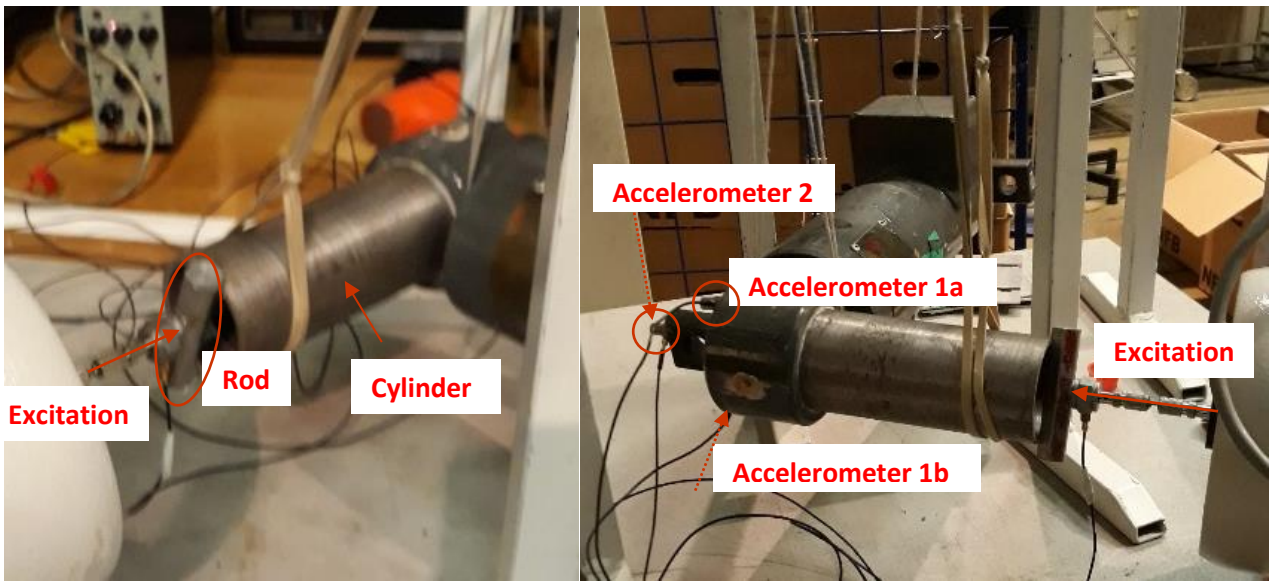

Figure 22: Dynamic stiffness measurement in Z-direction: location of the excitation point and accelerometers. The excitation force from the shaker acts on a stiff rod fixed to a hollow cylinder fixed to the casing. The acceleration of the casing is measured with two accelerometers (1a and 1b) to compensate for eventual rotation. Accelerometer 2 is located on the shaft.

It can be seen that the shaker applies the excitation in the middle of a rod, attached to a hollow cylinder which is in turn fixed to the casing. The accelerometer position on the casing and the shaft can be seen as well, although accelerometer 1b is not visible in the photograph.

3.4 MEASUREMENT RESULTS

The acceleration data is processed as indicated in Section 3.2 to obtain the acceleration transmissibility from the casing to the shaft and, based on this and on the estimated mass of the shaft (0.9 kg) the dynamic stiffness in the three Cartesian directions X, Y and Z is calculated. The result is provided in Figure 23, where the magnitude of the dynamic stiffness in N/m is plotted as a function of frequency, with the dynamic stiffness in the X-direction in blue, Y-direction in red and Z-direction in black. The loss factor, not shown, is found to be about 0.1 on average.

Above about 100 Hz, good results are obtained for the dynamic stiffness in the Z-direction, where the rubber is subject to pure shear motion. The frequency dependence is similar to the frequency dependence of the shear modulus of the rubber material [5] which means that the assumption that the thickness of the bushing is small compared to the wavelength is reasonable. Although for the X- and Y-directions some dynamic effects can be observed in the range 200-400 Hz, the results are satisfactory and agree with expectations. These dynamic effects are most likely due to bending vibrations of the lateral damper. The dynamic stiffnesses in the X- and Y-directions are very similar,

which implies that the bushing can be considered to be axi-symmetric and the casing of the bushing can be assumed to be infinitely stiff. Furthermore the stiffness increase in X,Y directions as at higher frequencies indicates that the damper is moving towards an anti-resonance outside the frequency range of interest.

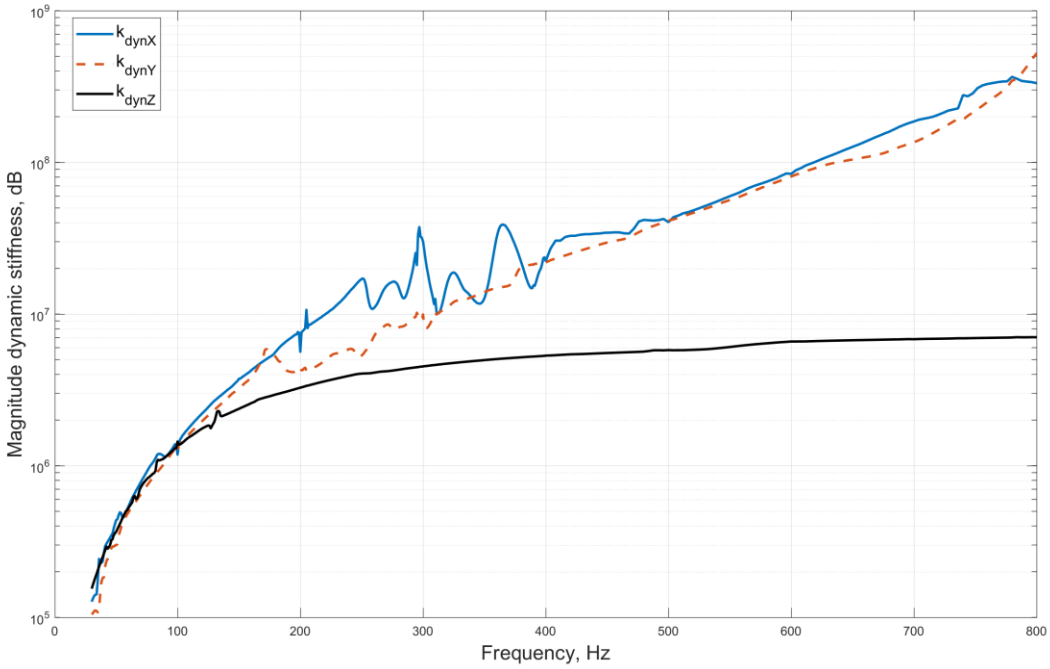

Figure 23: Dynamic stiffness of the bushings of the lateral damper bar. X-direction (blue dashed), Y-direction (red), Z-direction (black).

The results below 100 Hz for all three directions are not reliable. The stiffness estimation is based on a ratio of accelerations (T), both of which tend to zero as the frequency goes to zero. Therefore in the low frequency range the estimation is based on the ratio of two small quantities that, furthermore, tends to 1. Since the denominator in the expression for the dynamic stiffness is $T - 1$, small measurement errors can lead to large estimation errors. The measurement accuracy at low frequencies could be improved by attaching an additional mass to the outer ring of the bushing.

3.5 CONCLUSIONS

In this section measurements for the dynamic stiffness have been carried out on the bushing of the lateral damper from the Metro de Madrid Series 8000 vehicle. The method for the measurement for the dynamic stiffness for rubber bushings is described and applied to the estimation of the dynamic stiffness of the bushings of the lateral damper. Furthermore, the measurement set-ups for the lateral (X,Y) and axial (Z) directions are described and the measurement results are presented.

It can be concluded that the proposed method leads to a satisfactory estimation of the dynamic stiffness with a relatively simple measurement and calculation procedure. Therefore, the bushings of the lateral damper can be modelled as massless springs with frequency dependent stiffness characteristics.

4. TRACTION BAR

4.1 INTRODUCTION

In this section the measurements performed on the traction bar in the Metro de Madrid Series 8000 vehicle are described. Two sets of measurements have been carried out:

- Experimental modal analysis of the traction bar to identify its modal properties: modal frequencies, modal damping and modeshapes.
- Estimation of the dynamic stiffness of the bushings of the traction bar. These bushings have been provided as separate components and are tested independently of the traction bar itself.

4.2 EXPERIMENTAL MODAL ANALYSIS TRACTION BAR

4.2.1 Measurement apparatus

The following equipment is used for the measurements;

- Impact Hammer with Force transducer B&K type 8200, S/N 1895664
- Accelerometer – B&K type 4394V (2.4 g), S/N 1929297
- Charge amplifier – B&K type 2635, S/N 1799669
- 4-ch. Signal analyzing system Siglab, DSP Technology, S/N 11315

The experimental modal analysis is performed with a fixed accelerometer and a moving excitation (hammer with force transducer) by making use of the reciprocity principle, as described in detail in the next section.

4.2.2 Measurement set-up and procedure

In the first test the bar is placed on rubber isolators (Figure 24), since in practice the two ends are connected to bushings and other related parts. Two independent analyses are made for the two bending directions: Z-direction, with the traction bar resting on the flat side (Figure 24-(a)) and X-direction, with the traction bar resting on the round side (Figure 24-(b)). 13 basic points are marked for each surface, with point 7 in the middle of the bar. The distance between points is 0.02 m (Total length of the bar, including the bushing houses, is 0.553 m). An accelerometer is always fixed at

point “2” with the excitation (hammer) moving over all points. Thirteen transfer functions between force and acceleration are hence obtained for the analysis for each direction.

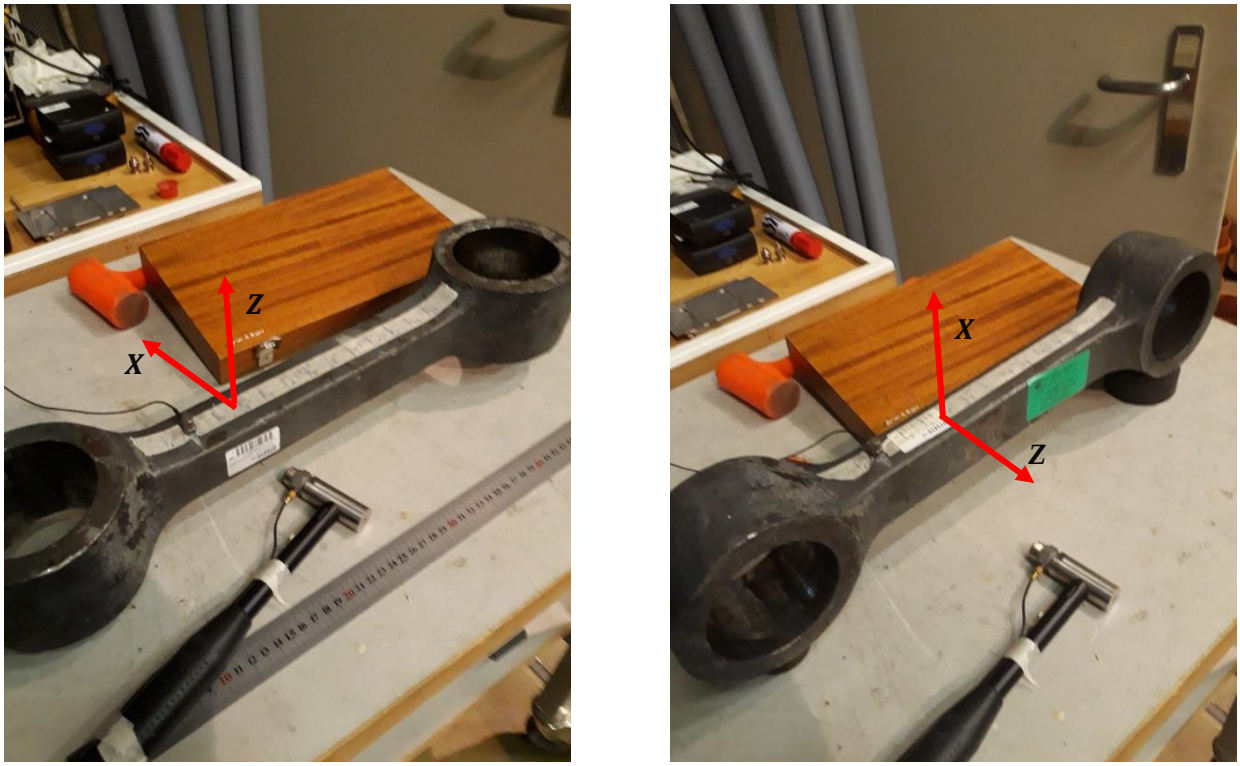

(a) (b)

Figure 24: First test with two ends (bushing houses) supported by rubber isolators. (a) Measurement in Z-direction, (b) Measurement in X-direction.

Results of modal analysis show that the beam modes of a free-free bar may have very important contributions to the vibration of the bar. A second test is then arranged, where the bar is freely-hanging by using two strings, see Figure 25. (Due to the weight of the bar, it is impossible to use ordinary rubber belts.) For the second arrangement, two extra points, at the surface of the bushing house (marked white), are used in each end when the bar is placed horizontally (measurement in Z-direction) as shown in the figure, hence the total number of the points becomes 17. For the X-direction there is one extra point at each end, on the highest point of the bushing house (also marked white in the figure). The total number of the points in this case is 15.

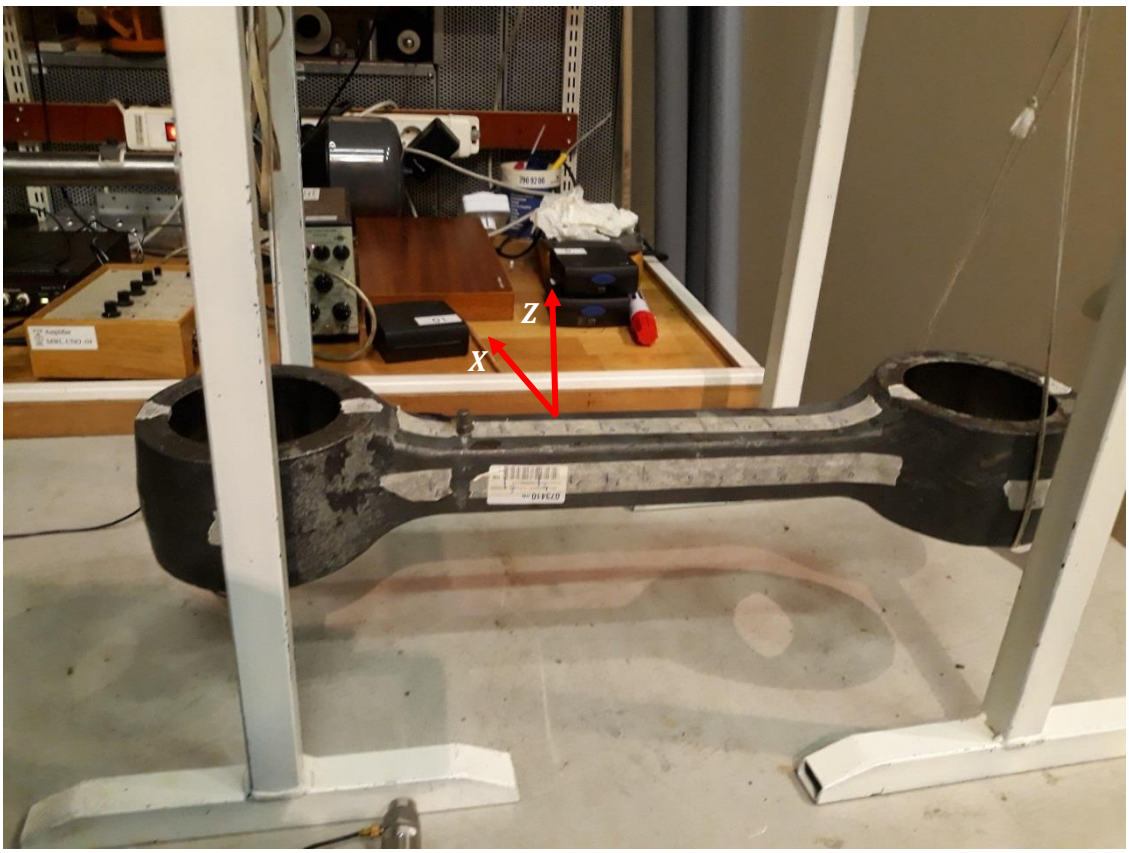

Figure 25: Freely hanging bar with position of the measurement point, position 2.

The point-accelerance for excitation at point 2 and response at point 2 and the corresponding coherence function are given in Figure 26: Z-direction results at position 2 of free-free hanging traction bar. (a) Point accelerance (dB re 1 m/s^{2}N), (b) CoherenceFigure 26 for excitation and response in Z-direction (see Figure 25 for the direction definitions) and Figure 27 for excitation and response in X-direction. The first three resonance frequencies in each direction are shown and the coherence values indicate that the quality of the point-accelerances is good. It can be seen that the resonance peaks are very lightly damped and even though a rather fine resolution is used (0.7 Hz), it is not sufficient for an accurate estimation of the loss factor.

In Table 2 the estimated values for the natural frequencies and loss factors for the first three modes in each direction are given. The first and third modes in each direction are the first and second bending modes, while the second mode is most likely the torsion mode, which is excited in both excitation directions. Although the loss factors found are very low, they are still over-estimated.

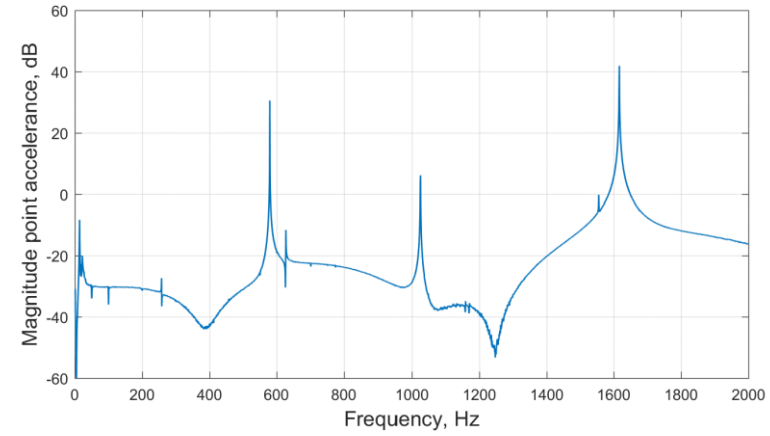

(a)

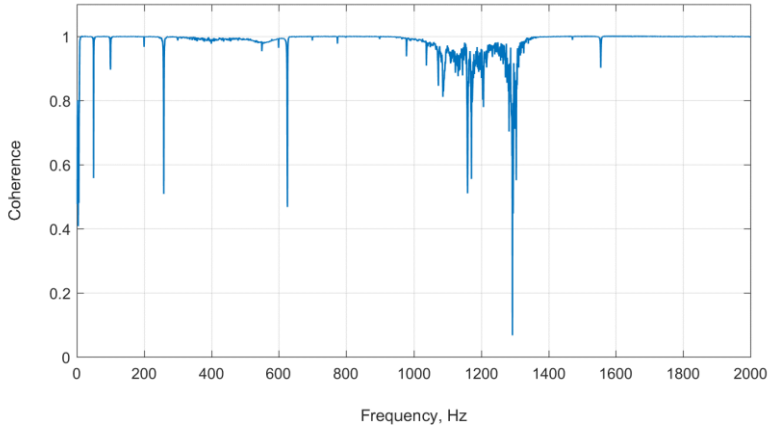

(b)

Figure 26: Z-direction results at position 2 of free-free hanging traction bar. (a) Point accelerance (dB re 1 m/s^{2}N), (b) Coherence

Table 2: Modal parameters for freely-hanging bar. Left: Z-direction, Right: X-direction

Bending in X-direction		Bending in Z-direction	
Resonant frequency (Hz)	Loss factor η	Resonant frequency (Hz)	Loss factor η
579.4	0.0004	627.2	0.00056
1025.5	0.00068	1024.8	0.00034
1615.3	0.00043	1555.1	0.00065

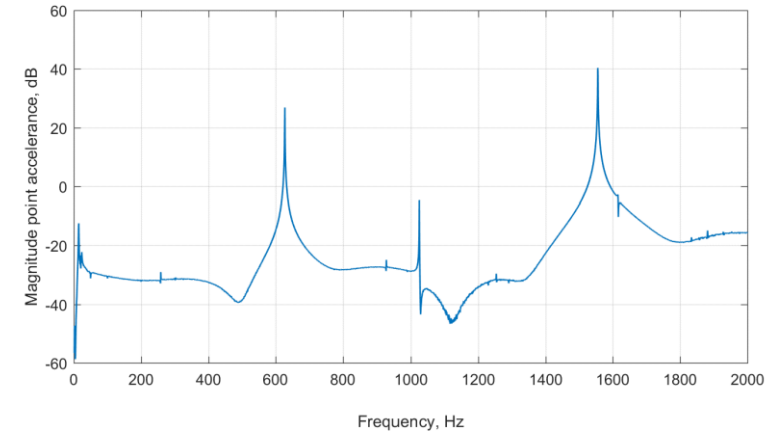

(a)

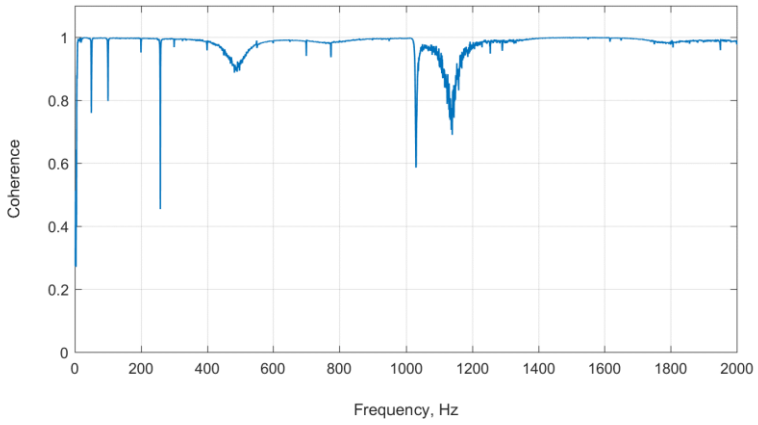

(b)

Figure 27: X-direction results at position 2 of free-free hanging traction bar. (a) Point accelerance (dB re 1 m/s^{2}N), (b) Coherence

In order to get a more accurate value for the loss factors, an estimation based on time decay-rates has been performed leading to the results summarized in Table 3. As expected the loss factors are even lower than estimated in the modal analysis and in agreement with the values that could be expected for a bar of solid forged steel. It should be kept in mind that in practice the loss factor of the traction bar will be dominated by the mountings on both sides of the bar and will be several orders of magnitude higher.

Table 3: Loss-factor in octave-bands based on time decay rate measurements

Center frequency (Hz)	250	500	1000	2000
Loss factor	0.0002	0.00021	0.00022	0.0006

4.3 DYNAMIC CHARACTERIZATION OF BUSHINGS

The dynamic stiffness of the bushings of the traction bar is obtained following the procedure used for the bushings of the lateral dampers that is described in Section 3. The same measurement method and measurement apparatus is used here. The mass of the shaft is estimated following the same procedure as before leading to an estimated mass of 1.68 kg.

The measurements are performed with the stepped sine method, i.e., excitation and measurements are performed at a single tone at a time, in the frequency range 30 Hz – 800 Hz. The frequency step is 1 Hz between 30 and 400 Hz, and 4 Hz between 400 and 800 Hz. In total 471 frequency points are measured.

4.3.1 Set-up for the measurement of the lateral dynamic stiffness

The set-up for the measurement of the lateral (X,Y) dynamic stiffness is shown in Figure 28.

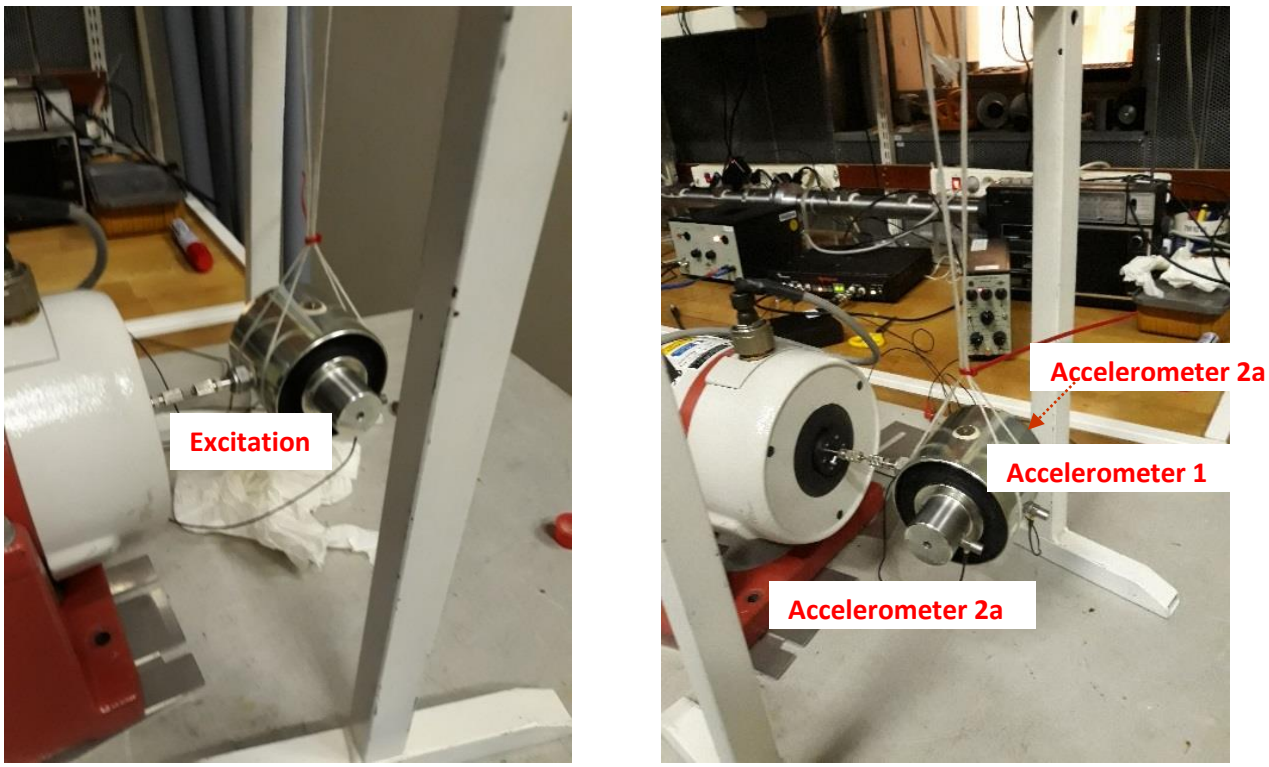

Figure 28: Dynamic stiffness measurements in X and Y-directions: location of the excitation point on the casing and the accelerometers on the casing (accelerometer 1) and on the shaft (accelerometer 2). The acceleration of the shaft is measured with two accelerometers (2a, 2b) to compensate for rotation.

The measurements are performed in two perpendicular directions to obtain the dynamic stiffness values in the X- and Y-directions, but, due to the axi-symmetry of the bushing, it leads to identical photographs. As before, two accelerometers are used to measure the acceleration of the shaft and the average value of the two is calculated in order to cancel out rotational vibrations.

4.3.2 Set-up for the measurement of the axial dynamic stiffness

The set-up for the measurement of the axial dynamic stiffness (Z-direction) is shown in Figure 29.

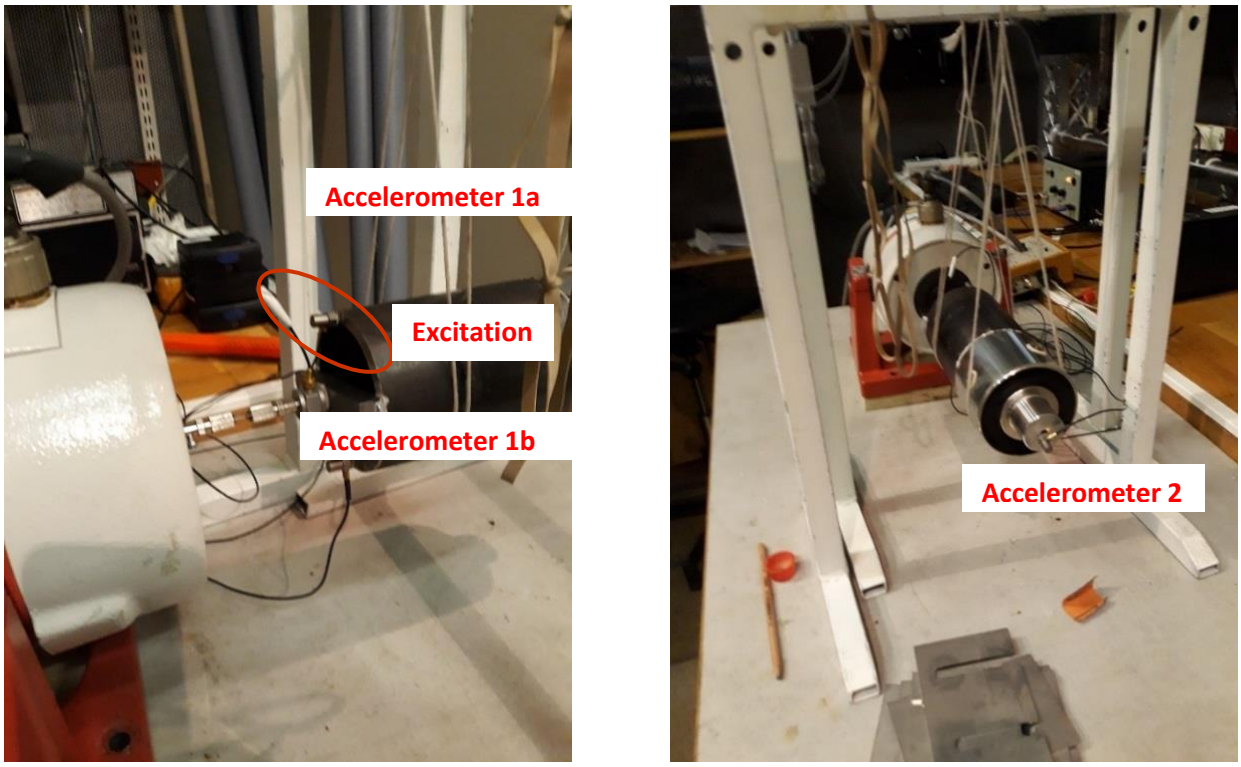

Figure 29: Dynamic stiffness measurement in Z-direction: location of the excitation point and accelerometers. The excitation force from the shaker acts on two points on the casing through a brace. The acceleration of the casing is measured with two accelerometers (1a and 1b) to compensate for eventual rotation. Accelerometer 2 is located on the shaft.

As in the case of the bushing of the lateral damper, the excitation force is applied through a hollow cylinder attached to the casing and the acceleration of the casing is obtained as the average of acceleration measurement at two symmetric positions.

4.3.3 Measurement results

The acceleration data is processed as indicated in Section 3.2 to obtain the acceleration transmissibility from the casing to the shaft and, based on this and on the estimated mass of the

shaft (1.68 kg), the dynamic stiffness in the three Cartesian directions X, Y and Z is calculated. The result is provided in Figure 30, where the magnitude of the dynamic stiffness in N/m is plotted as a function of frequency, with the dynamic stiffness in the X-direction in blue, Y-direction in red and Z-direction in black. The average loss factor is 0.1.

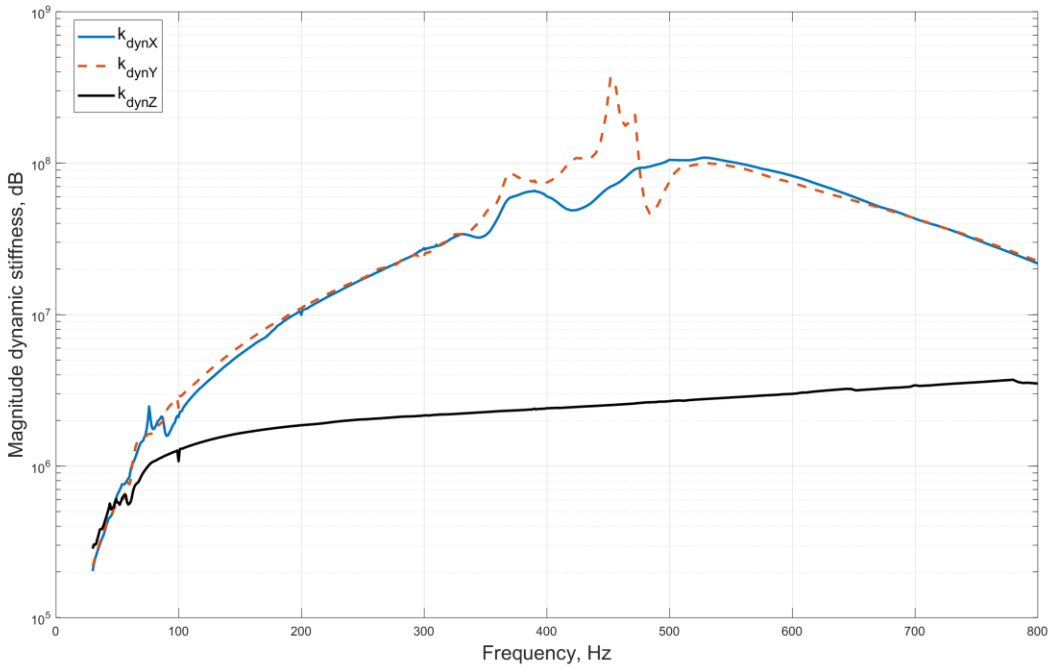

Figure 30: Dynamic stiffness of the bushings of the traction bar. X-direction (blue dashed), Y-direction (red), Z-direction (black).

Good results are obtained for the dynamic stiffness in the Z-direction, where the rubber is subject to pure shear motion. As in the previous section, the frequency dependence of the stiffness is similar to the frequency dependence of the shear modulus of the rubber material [5], which indicates that wave motion in the rubber can be neglected. Although for the Y-direction some dynamic effects can be observed in the range 350-500 Hz, most likely due to misalignments, the results are satisfactory and agree with expectations. As expected, the dynamic stiffness in the X- and Y-directions are very similar due to axi-symmetry. The decrease in stiffness above 500 Hz seems to be due to the test object moving towards a resonance in the high frequencies outside frequency range. The results below 100 Hz for all three directions are not reliable. The stiffness estimation is based on a ratio of accelerations, both of which tend to zero as the frequency goes to zero. Therefore in the low frequency range the estimation is based on the ratio of two small quantities and small measurement errors can lead to large estimation errors.

4.4 CONCLUSIONS

In this section the experimental characterization of the traction bar from the Metro de Madrid Series 8000 vehicle is discussed, including an experimental modal analysis of the traction bar and the estimation of the dynamic stiffness of the bushings. The measurement methods used are described and the results are presented.

The experimental modal analysis based on hammer measurements and the reciprocity principle (fixed accelerometer position and moving excitation point) leads to satisfactory results. However, the loss factors found are very low, purely due to material damping, and are not representative for damping in the traction bar in the real operating conditions, where the energy losses will be dominated by the bushings and by friction at the connections.

Furthermore, the method for the estimation of the dynamic stiffness presented in Section 3 is applied to obtain the dynamic stiffness of the bushings of the traction bar, leading to satisfactory results in the frequency range of interest. It is concluded that the bushings of the traction bar can be modelled as massless springs with a frequency dependent stiffness characteristic.

5. CONCLUSIONS

In this report the dynamic properties of suspension elements of the Metro de Madrid Series 8000 vehicle are measured and models to describe their behaviour are proposed.

Measurements for the static and dynamic stiffnesses have been carried out for the primary suspension spring. The static stiffness was found to be relatively constant at about 0.5 MN/m for preloads up to about 20 kN, above which it increases to about 1.4 MN/m at 39 kN. The vertical and lateral dynamic stiffnesses were measured using the indirect method with preloads applied between 10 and 40 kN. For the vertical dynamic stiffness, the magnitude at low frequencies is about 1 MN/m. There are two peaks caused by the internal resonances at around 200 and 450 Hz. Both the peak frequency and level increase with increasing preload. For the lateral stiffness, a higher magnitude of about 5 MN/m is found at low frequencies, and the first resonance peak occurs at around 450 Hz.

A model based on a mass-spring system including wave motion in the rubber elements has been developed. Good agreement with the measurement has been obtained for both the vertical and lateral stiffness in terms of the magnitude and the phase. Both the internal resonance frequency and the magnitude of the peak can be well predicted.

The experimental modal analysis of the traction bar based on hammer measurements and the reciprocity principle (fixed accelerometer position and moving excitation point) leads to satisfactory results. However, the loss factors found are very low, purely due to material damping, and are not representative for damping in the traction bar in the real operating conditions, where the energy losses will be dominated by the bushings and by friction at the connections.

A method for the measurement for the dynamic stiffness for rubber bushings is described and applied to the measurement of the dynamic stiffness of the bushings of the lateral damper and the traction bar. In order to obtain an estimation of the dynamic stiffness, an approximate model of the bushing is used, where the wave motion in the rubber is neglected and the bushing is modelled as a massless spring with a frequency dependent stiffness, while the casing is modelled as a massive rigid body. It is concluded that the proposed method and model lead to satisfactory estimations of the dynamic stiffness with a relatively simple measurement and calculation procedure. Therefore, the bushings of the lateral damper and traction bar can be modelled as massless springs with frequency dependent stiffness characteristics.

REFERENCES

1. ISO 10846-3: 2002. Acoustics and vibration – laboratory measurement of vibro-acoustic transfer properties of resilient elements – part 3: indirect method for determination of the dynamic stiffness of resilient supports for translatory motion.

2. Thompson, D. J., Van Vliet, W. J., & Verheij, J. W, Developments of the indirect method for measuring the high frequency dynamic stiffness of resilient elements. *Journal of Sound and Vibration*, 213(1), 169-188, 1998.

3. Fahy, F., & Walker, J., Advanced Applications in Acoustics, Noise and Vibration. CRC Press, 2004.

4. Kari, L., Dynamic transfer stiffness measurements of vibration isolators in the audible frequency range. *Noise Control Engineering Journal*, 49(2):88-102, 2001.

5. Kari, L., Eriksson, P., Stenberg, B. Dynamic stiffness of natural rubber cylinders in the audible frequency range using wave guides, Kautschuk Gummi Kunststoffe, 54 106-113, 2001.